The Hg isoelectronic defect in ZnO

J. Cullen, K. Johnston, D. Dunker, E. McGlynn, D. R. Yakovlev et al.

Citation: J. Appl. Phys. **114**, 193515 (2013); doi: 10.1063/1.4832458
View online: http://dx.doi.org/10.1063/1.4832458
View Table of Contents: http://jap.aip.org/resource/1/JAPIAU/v114/i19
Published by the AIP Publishing LLC.

The Hg isoelectronic defect in ZnO

J. Cullen,[1] K. Johnston,[2,3] D. Dunker,[4] E. McGlynn,[1,a)] D. R. Yakovlev,[4,5] M. Bayer,[4] and M. O. Henry[1]

[1]*School of Physical Sciences, National Centre for Plasma Science and Technology, Dublin City University, Glasnevin, Dublin 9, Ireland*
[2]*PH Department, ISOLDE/CERN, 1211 Geneva 23, Switzerland*
[3]*Technische Physik, Universität des Saarlandes, 66041 Saarbrücken, Germany*
[4]*Experimentelle Physik 2, Technische Universität Dortmund, 44227 Dortmund, Germany*
[5]*Ioffe Physical-Technical Institute, Russian Academy of Sciences, 194021 St. Petersburg, Russia*

(Received 27 September 2013; accepted 5 November 2013; published online 21 November 2013)

We report a study of the luminescence due to Hg in ZnO, concentrating on the main zero phonon line (ZPL) at 3.2766(1) eV and its associated phonon sidebands. For a sample implanted with radioactive ^{192}Hg, the ZPL intensity, normalised to that of shallow bound exciton emission, is observed to decrease with an equivalent half-life of 4.5(1) h, very close to the 4.85(20) h half-life of ^{192}Hg. ZnO implanted with stable Hg impurities produces the same luminescence spectrum. Temperature dependent measurements confirm that the zero phonon line is a thermalizing doublet involving one allowed and one largely forbidden transition from excited states separated by 0.91(1) meV to a common ground state. Uniaxial stress measurements show that the allowed transition takes place from an orbitally degenerate excited state to a non-degenerate ground state in a centre of trigonal (C_{3v}) symmetry while the magneto-optical properties are characteristic of electron-hole pair recombination at an isoelectronic defect. The doublet luminescence is assigned to bound exciton recombination involving exchange-split Γ_5 and $\Gamma_{1,2}$ excited states (using C_{6v} symmetry labels; Γ_3 and $\Gamma_{1,2}$ using C_{3v} labels) at isoelectronic Hg impurities substituting for Zn in the crystal. The electron and hole g values deduced from the magneto-optical data indicate that this Hg impurity centre in ZnO is hole-attractive. © *2013 AIP Publishing LLC*. [http://dx.doi.org/10.1063/1.4832458]

I. INTRODUCTION

Oxides in the solid state encompass a wide range of material types, from highly insulating through semiconducting to metallic (and transitions between such states), no less remarkable than the range of types exhibited by other material systems such as the group IV elements and the III-V compounds.[1,2] Furthermore, oxides have current applications and future potential in diverse areas that include catalysis, solar energy, optoelectronics, and spintronics, for example. This is also the case for nano-scale oxides, which have been the subject of extensive and sustained research in the recent past.[3–5] Whatever the application, the fundamental material science always determines the ultimate applicability of a material system in a technology area. In this paper, we are concerned with the fundamental properties of a single atom impurity defect in ZnO, one of the most widely studied oxides due to its current applications and future potential as a platform for optoelectronic and spintronic technologies. For such applications, point defects that interact with electrons and holes have roles that can vary from essential to the successful application of the material to being the *bêtes noires* that can undermine otherwise promising routes to a successful technology, and thus understanding the physics of point defects remains a key challenge.

It is instructive to compare the case of II–VI oxides with the III–V material systems. The majority of the latter possess the zincblende structure, for which the full range of mixed compositions is possible, such that these materials are widely used in band gap engineering of emitters and detectors. In the case of II–VI compounds, however, the crystal structures of the oxides of the group IIb elements Zn, Cd, and Hg vary from hexagonal (ZnO) to cubic (CdO) to orthorhombic/hexagonal (HgO), which is a much more complicated situation. Given these very different crystal structures, even the case of a single isolated impurity raises important questions regarding how the metal impurity will bond to its neighbouring atoms in the crystal, how the impurity affects its local environment and the optoelectronic properties of the material.

In this work, we report our studies of the case of isolated single Hg impurity atoms substituting for Zn in ZnO, which are expected to act as isoelectronic impurities. Such impurities form an important class of impurity systems for semiconductors because of their ability to act as binding centres for excitons, leading to efficient optical emission in many materials due to the absence of non-radiative processes such as Auger recombination.[6,7] The ZnO:Hg system has been reported by Agne *et al.*[8] to produce a doublet zero-phonon line (ZPL) emission in photoluminescence (PL) with the main line at 3.2765 eV and a much weaker line ~0.9 meV lower in energy, and with associated phonon sidebands of both lines to lower energies. These authors speculated, without supporting data, that the PL was due to the recombination of isoelectronic bound excitons (which we denote IBX in keeping with bound exciton notation in the ZnO literature)

a)Author to whom correspondence should be addressed. Electronic mail: enda.mcglynn@dcu.ie

localised at Hg impurities. The ZnO:Hg IBX energy lies ~100 meV below the ZnO free exciton position, considerably deeper than the common donor bound exciton (DBX) lines which have binding energies typically in the range 10–20 meV.[9] There is only one other example of IBX recombination reported for ZnO, of unknown chemical origin, that produces PL emission at 3.3621 eV (Ref. 10) and which lies directly among the DBX lines, very different from the case of ZnO:Hg. Thus, confirmation of the isoelectronic nature of the ZnO:Hg emission and further study of the properties of isoelectronic defects is needed to more fully understand the behaviour of this important defect type and its bound exciton species in ZnO.

In the study by Agne *et al.*, radioactive ^{197}Hg (which has a half-life of 92.53 h) was used to confirm the identification of the PL with Hg.[8] In that study, the measurements were made over a period of 20 days, and, although the same measurement temperature of 1.6 K was used for all spectra recorded, the sample temperature cycled regularly between 1.6 K and 120 K between measurements.[8] In the present study, we use ^{192}Hg for which the half-life is only 4.85 h; this allows us to complete the measurements over approximately one day while maintaining the sample at the measurement temperature of ~4 K at all times. We also extend the scope of the investigation to include detailed temperature dependence measurements, and both uniaxial stress and magneto-optical measurements with a view to establishing the symmetry of the impurity centre and the nature of the bound exciton electronic states. Our results establish the IBX nature of the ZnO:Hg PL, and they enable us to identify the strong and weak ZPL transitions with IBX recombination involving exchange-split Γ_5 and $\Gamma_{1,2}$ states (using C_{6v} symmetry labels), respectively, of the IBX. The electron and hole g values deduced from the magneto-optical data indicate that the Hg impurity centre in ZnO is hole-attractive. We also note some surprising features in terms of the physics of this defect, first that the thermal binding energy obtained from the temperature dependence is much less than the spectral binding energy relative to the free exciton position, and also much less than is typical of a shallow donor system in ZnO and second that the departures of hole g-values (from free hole g-values) determined from Zeeman studies for this defect are much less than those seen for the only other reported isoelectronic defect in ZnO,[10] which was a more shallow defect, contrary to the pattern expected and generally seen for other defects in various materials. These unusual behaviours may be related to specific issues associated with defect electronic binding and structure due to the differing crystal structures of the oxides of Zn and Hg noted above.

II. EXPERIMENTAL

Hydrothermally grown single crystal samples of ZnO, obtained from Tokyo Denpa Ltd., were doped via ion implantation at the On-Line Isotope Mass Separator facility (ISOLDE) in the European Organisation for Nuclear Research (CERN) with ^{192}Hg (which decays via electron capture to ^{192}Au) at a nominal dose of 1×10^{13} ions cm^{-2} and an ion beam energy of 60 keV. Other samples using starting material from the same supplier were implanted with stable Hg at the University of Surrey using the same ion energy and dose. All samples were annealed in air at 750 °C for 30 min in order to remove residual implantation damage in the crystal. The sample dimensions were either $10 \times 10 \times 0.5$ mm^3 or $10 \times 4 \times 0.5$ mm^3.

The details of the spectroscopic equipment are similar to those described by Cullen *et al.*[11] In summary, PL emission was generated using the 325 nm line of a HeCd laser with an excitation density of ~200 mW/cm^2. For general measurements, the PL was analysed using a 1 m grating spectrometer (SPEX 1704 with a resolution of 0.01 nm) equipped with a photomultiplier tube (Hamamatsu model R3310-02) in photon counting mode and cooled by a Peltier system EMI FACT50 cooler to approximately −20 °C. An iHR320 spectrometer with a resolution of 0.07 nm was used to record spectra of samples under uniaxial stress; the detector was a Peltier-cooled Andor Newton electron multiplying CCD cooled to −30 °C. For PL measurements at the ISOLDE facility in CERN, the PL was analysed by a SPEX 0.75 m grating spectrometer with a resolution of 0.01 nm equipped with a liquid nitrogen cooled Jobin-Yvon CCD detector. In all cases, closed cycle cryostats (either a SHI-950-5 or SHI-950, both from Janis Corporation) were used to cool the samples to temperatures in the range 3–20 K.

Magneto-optical measurements were made using a split-coil magnet cryostat from Oxford Instruments generating magnetic fields up to 7 T; as an excitation source, the second harmonic (using a lithium triborate, LiB_3O_5 (LBO), crystal) of an optically pumped (Verdi 10 W laser from Coherent) Ti:Sapphire laser from Tekhnoscan was used with a wavelength of 355 nm and ~50 mW power, and the PL was analysed with a Horiba U1000 double monochromator, at a resolution of 0.01 nm, equipped with a R943-02 Hamamatsu photomultiplier tube. Sample temperatures in the range 5–10 K were used in the magneto-optical measurements.

For uniaxial stress measurements, vertically aligned samples were mounted in shallow slots cut to the thickness of the samples in the faces of two stainless steel pistons in a stress apparatus described in Ref. 12. A piezoelectric load cell (Bofors KRA-1) produced an output voltage proportional to the force applied on the sample through a push rod. A steel ball-bearing was used at the base of the load cell to transfer the force of the spring loading mechanism without transferring the twisting motion of the threaded bar to the piston. The sample temperature during the uniaxial stress measurements was 10 K.

III. RESULTS

A. Photoluminescence

A composite PL emission spectrum of ZnO implanted with stable ^{199}Hg is shown in Fig. 1(a). The usual DBX lines and their two electron satellite (TES) lines are prominent in the spectrum and, in addition, as previously reported by Agne *et al.*[8] for ZnO:^{197}Hg, a sharp ZPL emission is observed at 3.2765 eV (which we denote as the A-line below in keeping with the notation used in Ref. 8) along with an associated phonon sideband at lower energies. A series of spectra for a radioactive ZnO:^{192}Hg sample, recorded over

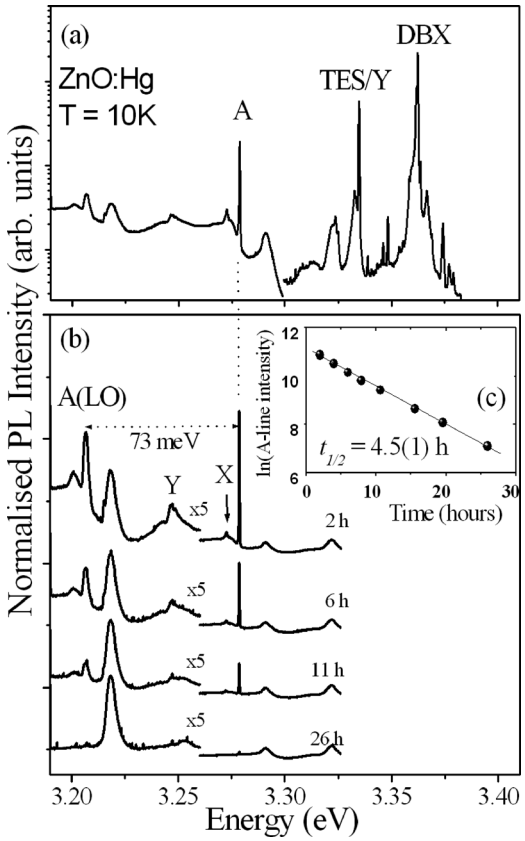

FIG. 1. Representative PL spectrum (a) showing the ZnO spectra after implantation of stable Hg. The Hg-related ZPL A-line is observed at 3.2766(1) eV and an associated LO phonon replica 73 meV lower in energy than the A-line. In (b) and (c) the A-line in a sample implanted with radioactive ^{192}Hg is seen to decrease with a calculated half-life of 4.5 ± 0.2 h, very close to the tabulated half-life of ^{192}Hg (4.85 h). Spectra are vertically stacked for clarity.

the course of five half-lives of ^{192}Hg, normalized to the intensity of the DBX lines $I_{6/6A}$ which were observed not to change significantly with time, are shown in Fig. 1(b) in which the decreasing intensity of the A-line as the ^{192}Hg decays to ^{192}Au is clearly evident. In Fig. 1(c), we show a graph of the natural log of the normalized A-line intensity as a function of time after annealing. The linear fit to the data corresponds to an equivalent half-life of 4.5(1) h for the A-line intensity, which agrees very well with the 4.85(20) h half-life of ^{192}Hg. We conclude, in agreement with Ref. 2, that the ZPL is due to Hg and that it involves single isolated Hg impurity atoms in the ZnO crystal.

A comprehensive analysis of the phonons contributing to the sidebands in the ZnO:Hg IBX is given in Ref. 8 and we do not repeat that detailed analysis here. We note only the three prominent features labelled X, Y, and A(LO) in Fig. 1(b), at separations of 6.4, 32, and 73 meV, respectively, from the ZPL at 3.2766(1) eV. The X feature is attributed to the creation of a low energy local mode phonon, while the Y feature is assigned to a ZnO optical mode phonon[8] and the 73 meV feature results from the creation of an LO phonon in the recombination process. Overall, the intensity of the phonon sidebands relative to the ZPL results in an estimate of 0.7 for the Huang-Rhys phonon coupling parameter S, significantly larger than the value of approximately 0.2 observed for the DBX lines.[13]

The temperature dependence of the PL was also measured. The doublet nature of the ZPL is confirmed by the spectrum in Figs. 2(a)–2(d) which shows that the dominant A-line is accompanied by a weaker line labelled B at 3.2756 eV, at a separation of 0.91(1) meV from the A-line. The data in Fig. 2(e) show that the thermalisation energy for the two lines corresponds within the fit error to the spectroscopic separation, thereby confirming that they share a common ground state. The extrapolation to infinite temperature of the intensity ratio data in Fig. 2(e) shows that the radiative efficiencies, neglecting any degeneracy difference for the two excited states, are in the ratio A:B ∼ 400:1. This result means that a strong selection rule governs the two transitions, with the B-line being due to essentially forbidden transitions. Although we have observed weak emission unrelated to the ZnO:Hg IBX spectrum in some ZnO samples close to the position of the B-line, the occurrence of an essentially forbidden transition ∼0.9 meV below the A-line is unequivocally confirmed by magneto-optical data to be presented and discussed below.

The temperature dependence of the A-line intensity as a function of inverse temperature is plotted in Fig. 2(f) for temperatures in the range 3–40 K. The initial increase as the temperature is raised from 3 to ∼10 K is due to the increasing population in the initial state of the (allowed) A-line, as noted above. The intensity is relatively stable over the range 10–15 K but then falls off rapidly as the temperature increases further. This rapid loss is due to the thermal breakup of the IBX from the Hg impurity. The full temperature dependence of the A-line intensity can be described by the equation

$$I_A(T) \propto \exp(-\Delta E_{AB}/k_B T)/(1 + \exp(-\Delta E_{AB}/k_B T\, k_B T) + rT^{3/2}\exp(-E_b/k_B T)),$$

where ΔE_{AB} is the energy separation of the A and B lines, E_b is the IBX confinement energy, and the factor $rT^{3/2}$ takes account of the temperature dependent ratio of the density of band states relative to the concentration of Hg impurity atoms in the crystal. For the fit shown by the solid line in Fig. 2(f), we set $\Delta E_{AB} = 0.9$ meV, the observed A-B spectroscopic separation, and the other fit parameters are $E_b = 12.2$ meV and $r = 32$. The IBX thermal binding of ∼12 meV is quite small despite its large spectral binding energy relative to the free exciton position.

Further confirmation of both thermalisation between the A and B lines and the identification of the LO phonon replicas with these ZPL is found by studying the shape and position of the LO replica of the lines in comparison to the ZPL spectra. In Fig. 3(a), the two ZPL features can be seen, the A-line only at 10 K and the B-line dominating at 2 K. In Fig. 3(b), the corresponding LO replica emission of each line can be seen 73 meV lower in energy; the phonon sidebands of both ZPLs also look very similar. Note also in Fig. 3(a) that the position and shape of the "X" phonon sidebands of the A and B lines change between 2 and 10 K, due to the changing populations of the two excited states between those temperatures.

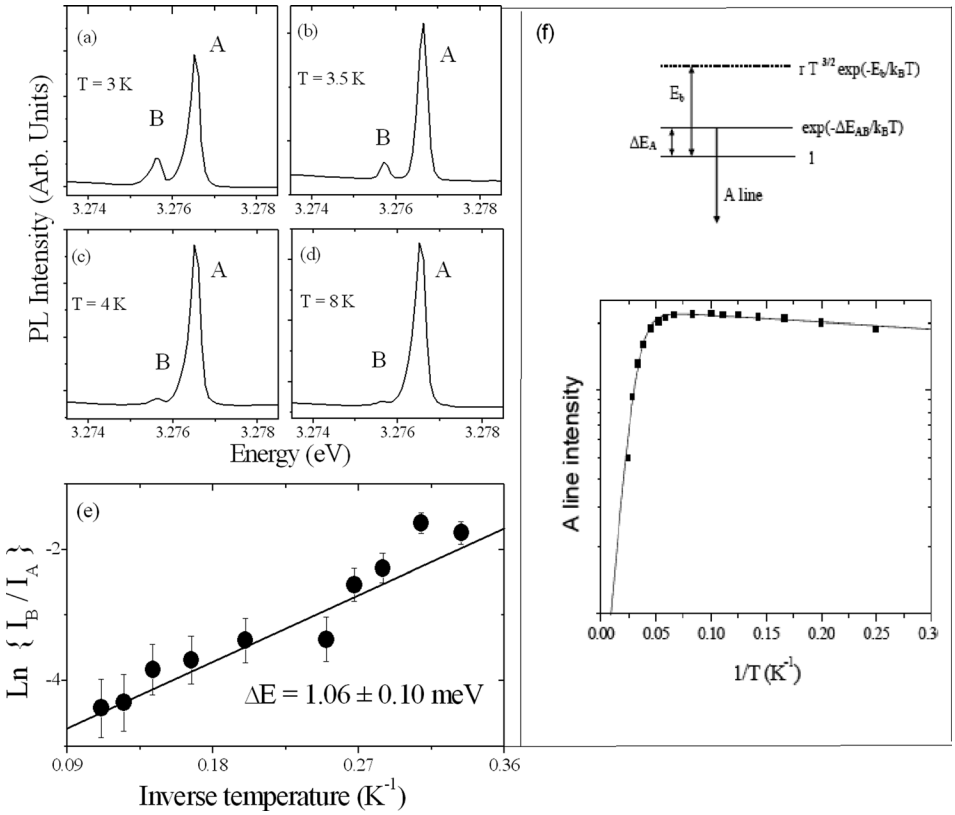

FIG. 2. PL spectra (a) to (d) of the Hg ZPL doublet, consisting of a higher energy A-line and a lower energy B-line for temperatures in the range 3 to 8 K. Temperature dependent relative intensities (e) confirm that there is thermalisation between the A- and B-lines. In part (f), the temperature dependence of the A-line intensity for the range 3–40 K and a simple model to account for the observed dependence are shown.

B. Uniaxial stress

In order to investigate the symmetry of the defect centre, uniaxial stress measurements were performed for stress both parallel (along [0001]) and perpendicular (along [1-210] and [10-10]) to the c-axis. PL spectra for stress parallel to the c-axis, in Fig. 4(a), show that a linear shift of +3.95 meV/GPa is observed without any splitting. While no significant line broadening was observed for the A-line, a significant decrease in PL intensity is observed in contrast to the DBX lines which were observed to maintain their intensity under stress up to 1 GPa. The change in PL intensity under stress in the phonon sidebands is the same as that for the ZPL. For stress applied perpendicular to the c-axis, along the [1-210] direction, the A-line was observed to split into two components as shown in Fig. 4(b); one component moves to higher energies at a rate of +0.63 meV/GPa, while the other A-line component moves to lower energies at a rate of −1.11 meV/GPa. Note that the higher energy component gets weaker as the stress-induced separation increases; this indicates that the two components are thermalising at 10 K and consequently that the splitting under stress is due to the lifting of an electronic degeneracy in the excited state of the A-line.

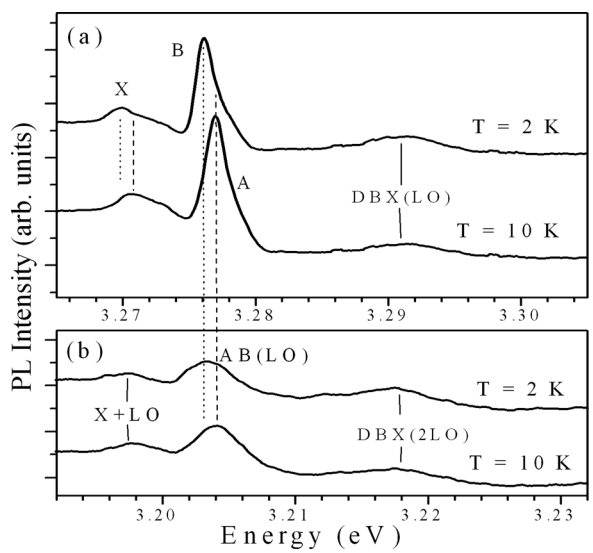

FIG. 3. (a) Zero phonon and local mode X sidebands of the ZnO:Hg A and B transitions. The A-line disappears almost entirely at 2 K where the "forbidden" B transition dominates. In (b), the first LO phonon replicas of the A, B, and X lines are shown. The spectra are shifted vertically for clarity.

Stress applied along the [10-10] direction, also perpendicular to the c-axis, results in a similar splitting pattern to that under [1-210] stress: the A-line splits into two thermalising components, one moving to higher energies at a rate of +0.67 meV/GPa and the other to lower energies at a rate of −1.37 meV/GPa. Representative spectra are shown in Fig. 4(c). The fan diagrams for the full set of A-line stress data are included in Fig. 4, panels (d), (e), and (f).

Regarding the effects of stress on the B-line, Fig. 4(a) shows that it has the same behaviour as the A-line for stress parallel to the c-axis. For stress parallel to the [10-10] direction (Fig. 4(c)), the line is clearly visible and a shift rate of −0.91 meV/GPa was obtained but without any splitting taking place. As the line was not observed for stress in the [1-210] direction, the data for the B-line are not complete so the stress analysis below deals with the A-line alone, although the lack of splitting of the B-line is consistent with the discussion and conclusions below.

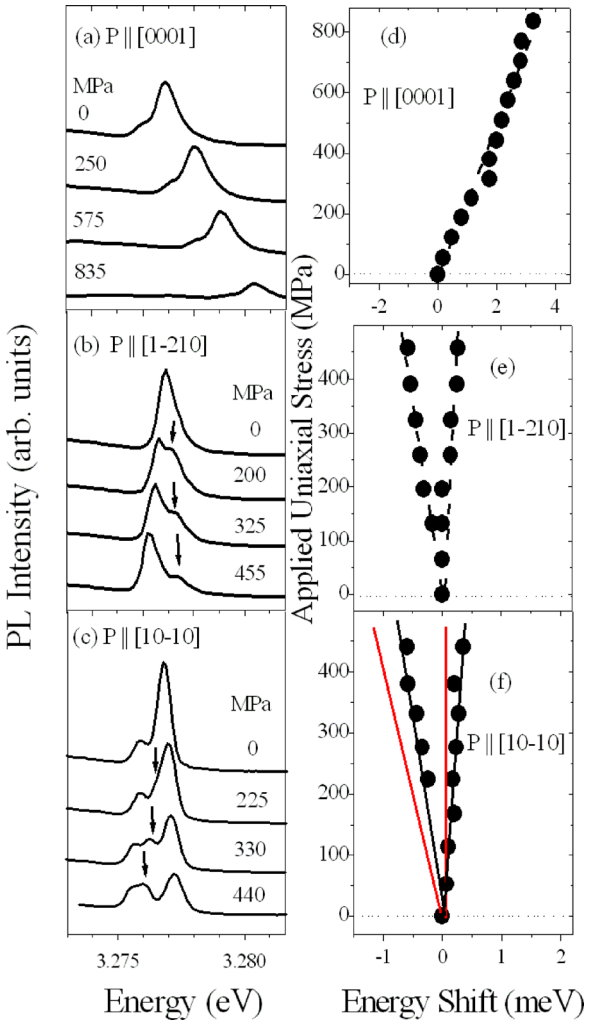

FIG. 4. PL spectra (a)–(c) and peak energy positions (d)–(f) of the Hg A-line for samples under uniaxial stress along the [0001], [1-210], and [10-10] directions. Black lines in (d)–(f) represent fits calculated for a $\Gamma_5(\Gamma_3)$ to Γ_1 transition at a trigonal (C_{3v}) defect. The red lines in (f) correspond to the calculated shift rates for the case of a monoclinic defect.

C. Zeeman spectroscopy

Note first that we use the symbol $\boldsymbol{B}$ for the magnetic field to avoid confusion with the PL line label B. PL spectra at 5 K for magnetic field values in the range 0 to 7 T are shown in Figure 5(a) for $\boldsymbol{B} \parallel \mathbf{c}$ and the electric vector of the luminescence $\mathbf{E} \perp \boldsymbol{B}$. The B-line is not observed for these conditions. For the A-line, while no splitting is observed for this geometry, a slight broadening is evident in Fig. 5(a) with the linewidth increasing by approximately 15%. Similarly, a slight broadening of ~5% is observed for the A-line, where $\boldsymbol{B} \parallel \mathbf{c}$ and $\mathbf{E} \parallel \boldsymbol{B}$ (not shown).

In Fig. 5(b), the spectra for $\boldsymbol{B} \perp \mathbf{c}$ and $\mathbf{E} \parallel \boldsymbol{B}$ are shown. In this case, the B-line, though not present at zero field, becomes the dominant feature at the higher magnetic fields. Additionally, the A-line is found to split into two components labelled A and A*. Similar spectra were obtained for the electric vector of the light perpendicular to the magnetic field (not shown).

The temperature dependance of the A- and B-line intensities observed for $\boldsymbol{B} \perp \mathbf{c}$ is shown in Fig. 6(a) for $\boldsymbol{B} = 7$ T. It is immediately evident that the three lines

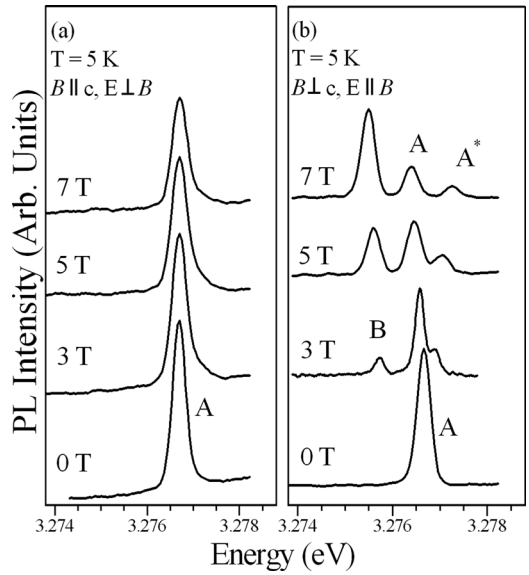

FIG. 5. PL spectra recorded with a magnetic field aligned parallel (a) and perpendicular (b) to the c-axis. In (b), the A-line is seen to split into two components and the B-line intensity increases strongly with increasing magnetic field.

thermalise, with the intensity shifting systematically to the higher energy lines at the expense of the lower energy lines as the temperature is raised, and this is confirmed by Arrhenius plots of the data. This indicates that the splitting is due to the lifting of degeneracy in only the excited states of the transitions and therefore that the ground state is non-degenerate, in full agreement with the findings of the uniaxial stress measurements.

The dependence of the B-line intensity on the magnitude of the magnetic field $\boldsymbol{B} \perp \mathbf{c}$ is plotted in Fig. 6(b), where we show the ratio of the integrated intensity of the B-line relative to that of the A-line as a function of $|\boldsymbol{B}|^2$ on a log-log plot. The linearity of the graph shows that the dependence on $|\boldsymbol{B}|$ is quadratic, confirming that a field-induced mixing of states causes the B-line to grow in intensity in the spectrum.

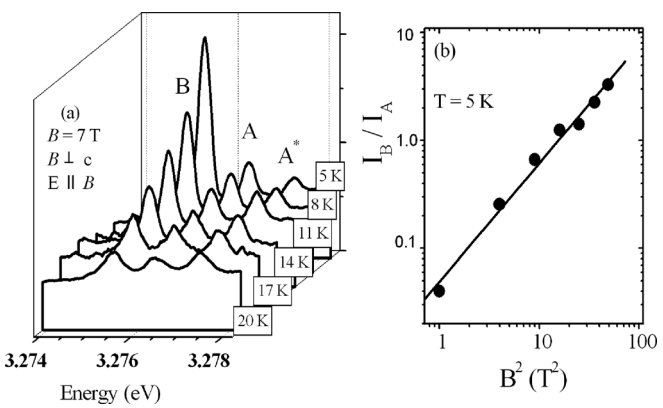

FIG. 6. The temperature dependence of the ZnO:Hg PL emission for a magnetic field of 7 T applied perpendicular to the c-axis is shown in part (a). In part (b), the ratio of the intensity of the B-line to the total intensity in the two A-line components is plotted as a function of the square of the magnitude of the applied magnetic field.

IV. DISCUSSION

We begin the discussion of results with a brief summary of our main findings regarding the general properties of the ZnO:Hg IBX spectrum, which substantially enhance and extend those previously reported by Agne *et al.*[8] First, the close agreement between the rate of the decrease of the A-line PL intensity for radioactive ^{192}Hg with the isotopic half-life proves that the defect involves a single Hg atom. Second, the occurrence of a closely spaced doublet in the ZPL involving one strong and one weak line (A and B, respectively) due to a split excited state is positively confirmed, with the added information that the oscillator strength ratio between the allowed and "forbidden" lines (neglecting degeneracies) is approximately 400:1. The phonon sidebands of the A and B lines are shown to have essentially the same form, with both lines having a low energy resonance of 6.4 meV in the sidebands and similar lattice phonon sidebands including a strong LO replica. The overall ratio of sidebands to ZPL produces an estimate of ~0.7 for the Huang-Rhys parameter S for the ZnO:Hg IBX, considerably larger than is typical of DBX lines in this material.[8] Thus, from a general spectroscopic perspective, the overall PL properties of the ZnO:Hg IBX are well understood. As noted by Agne *et al.*,[8] their provisional identification of the ZnO:Hg PL as being due to IBX recombination required further experimental verification, and we now discuss other results which provide comprehensive evidence on that point.

A. Uniaxial stress data analysis

The main findings in the uniaxial stress measurements reported in Fig. 4 above were that the A-line does not split under stress parallel to the c-axis and that it splits into two components for stresses in two orthogonal high-symmetry directions perpendicular to the c-axis, with quite similar shift rates for the two stress directions. These general findings can be analysed in detail by applying the generic results for the shift rates of optical transitions in wurtzite crystals under stress reported by McGlynn and Henry.[14] These authors show that there are two situations that match the general stress behaviour of the ZnO:Hg A-line: (i) transitions between an orbitally degenerate state and a non-degenerate state at a defect of trigonal (C_{3v}) symmetry and (ii) transitions between two orbitally non-degenerate states at a defect of monoclinic symmetry. For the former, the line splitting for stresses perpendicular to the c-axis is due to the lifting of the orbital degeneracy in one of the states, while for the latter, the splitting results from the lifting of orientational degeneracy amongst equivalent defects. We noted regarding the data in Fig. 4 that the higher energy component of the A-line under stresses perpendicular to the c-axis gets weaker as the stress-induced separation increases and consequently that the splitting is due to an electronic degeneracy in the excited state. Therefore, the clear implication is that the A-line in the ZnO:Hg PL spectrum arises from transitions from an orbitally degenerate excited state to a non-degenerate ground state in a defect of trigonal (C_{3v}) symmetry. For the second possibility to apply, i.e., that the defect is monoclinic, a changing intensity ratio for the components of the A-line would require that a subset of the defects re-orient under stress at low temperatures, which, though not impossible, is unlikely. Further evidence to support the trigonal identification rather than the monoclinic comes from a quantitative analysis of the measured shift rates using the generic equations developed in the theory which we now describe.

The predicted shift rates for stresses along the three crystal directions used in this study in the notation of McGlynn and Henry[14] are given in Table I, in terms of conventional stress parameters. The fitting of the equations for the trigonal (C_{3v}) case to the data in Figs. 4(d)–4(f), shown by the dashed black lines in those figures, is consistent for all three data sets. From these fits, the values obtained for the stress parameters are $At1 = 1.17$, $At2 = 1.39$, and $Bt1 = -0.83$ in units of meV/MPa. The equations for the monclinic case produce a poorer overall fit to the three data sets, illustrated by the dashed red lines in Fig. 4(f). Accordingly, we conclude that the A-line is due to transitions from a degenerate excited state to a non-degenerate ground state in a centre of trigonal (C_{3v}) symmetry.

The origin of such a degenerate excited state for the ZnO:Hg IBX is readily explained. The normal starting point is to consider an exciton constructed from a Γ_7 conduction band electron and a Γ_7 valence band hole (using C_{6v} symmetry labels for the wurtzite crystal). The Γ_7 symmetry of both the electron and hole states produces three exciton states from the $\Gamma_7 \otimes \Gamma_7$ direct product, which are given as Γ_1, Γ_2, and Γ_5. When these states are considered for the case of an exciton bound at a defect with C_{3v} symmetry, standard compatibility tables[15] show that the C_{6v} states Γ_1, Γ_2, and Γ_5 transform as Γ_1, Γ_2 and Γ_3, respectively, in C_{3v} symmetry. Henceforth, we will label the twofold degenerate state as $\Gamma_5(\Gamma_3)$, giving both the C_{6v} and C_{3v} (in brackets) labels, reflecting the variance of usage of C_{6v} and C_{3v} notation in the literature.[16–18] The Γ_1 and Γ_2 states, which typically lie lower in energy than the $\Gamma_5(\Gamma_3)$ state by about 1 meV,[18–20] are usually treated together (and as degenerate) since no evidence of any splitting between them has been reported in ZnO, and the label $\Gamma_{1,2}$ is used for the composite state. The separation between $\Gamma_{1,2}$ and $\Gamma_5(\Gamma_3)$ is a result of the different alignment of electron and hole spins for the two cases. For $\Gamma_{1,2}$, the spins are aligned parallel, whereas for $\Gamma_5(\Gamma_3)$, the spins are aligned anti-parallel. The ground state after the recombination of the electron-hole pair is the crystal ground state Γ_1. Symmetry arguments show that, while the $\Gamma_5(\Gamma_3)$ to Γ_1 transitions are dipole allowed with a large oscillator

TABLE I. The linear shift rate equations for defects of trigonal and monoclinic symmetries under stresses along the [0001], [1-210], and [10-10] directions in terms of conventional stress parameters.[14]

Stress direction	Trigonal (C_{3v} symmetry labels) Γ_3 to Γ_1	Monoclinic (C_{1h} symmetry labels) Γ_1 to Γ_1
[0001]	$At1 + 2At2$	$Am3$
[1-210]	$At1 - At2 + Bt1$	$Am2$
	$At1 - At2 - Bt1$	$\frac{1}{4}(3Am1 + Am2)$
[10-10]	$At1 - At2 + Bt1$	$Am1$
	$At1 - At2 - Bt1$	$\frac{1}{4}(3Am2 + Am1)$

strength, Γ_1 to Γ_1 is dipole allowed for E || c but the transition has a very small oscillator strength as it requires a spin change $\Delta s = 1$, while Γ_2 to Γ_1 is a dipole forbidden transition.[21] The basic description of free excitons in ZnO presented above also applies to the states of electron-hole pairs bound at defect or impurity sites where no other free particle is present, as is the case for the Hg IBX studied here. Thus, we can explain the uniaxial stress data by attributing the A and B lines observed in the ZnO:Hg PL to the allowed $\Gamma_5(\Gamma_3)$ to Γ_1 and (largely) forbidden Γ_1 to Γ_1 transitions, respectively, of an IBX bound at Hg impurity centres. Although we do not have a full data set for the B-line, the absence of any splitting for the two cases where it is observed is consistent with this analysis.

B. Zeeman data analysis

The analysis of Zeeman data for bound excitons in II-VI crystals was first developed by Thomas and Hopfield[16] for the case of CdS, and the same approach has been applied successfully to various exciton systems in ZnO.[9,22,23] The observed effects are found to be dominated by the electron and hole spin with the result that, in general, the analysis can be done successfully using the $\Gamma_{1,2}$ and Γ_5 exciton states in the C_{6v} symmetry of the crystal instead of the local symmetry of the impurity, but we will maintain our practice of labelling the twofold degenerate state as $\Gamma_5(\Gamma_3)$. In brief, and as noted above, the exciton state wavefunctions involve electron and hole spins which are parallel for $\Gamma_{1,2}$ (the B-line) and anti-parallel for $\Gamma_5(\Gamma_3)$ (the A-line) and the observed line splitting is determined by the extent to which the electron and hole g values govern the line shifts under the action of the applied field. Our data are confined to the two limiting cases of $\boldsymbol{B}$ || **c** and $\boldsymbol{B}$ ⊥ **c** only, so in the absence of a full set of angular dependence data, our approach is to attribute effective g values (g_{eff}) to the exciton states for these limiting cases and from this (using also general findings from other ZnO studies) to estimate the electron and hole g values g_e and g_h. We allow for the hole g value to be anisotropic, using the normal symbols $g_{h||}$ and $g_{h\perp}$ for the two orientations of the $\boldsymbol{B}$ field relative to the **c**-axis. Furthermore, we assume that the sign of $g_{h||}$ in the case of ZnO:Hg is opposite to that of g_e, as has been found generally for excitons derived from the upper Γ_7 valence band in ZnO to date.

We consider the A-line first, for which there are data for both $\boldsymbol{B}$ || **c** and $\boldsymbol{B}$ ⊥ **c**, and in order to facilitate the discussion, schematic diagrams for the A-line transitions for the two cases are shown in Figs. 7(c) and 7(d). The recombining electron and hole have anti-parallel spins for the A-line, and it is clear from Fig 7(c) that the absence of any splitting for $\boldsymbol{B}$ || **c** is explained if the hole g value $g_{h||}$ is equal in magnitude and opposite is sign to the electron g value g_e. Therefore, for $\boldsymbol{B}$ || **c**, the A-line in ZnO:Hg has $g_{eff} \sim 0$ and $|g_e| \sim |g_{h||}|$. The slight broadening that is observed as the magnetic field $\boldsymbol{B}$ || **c** increases, evident in Fig. 5(a), can be accounted for if the magnitudes of the hole and electron g-values differ slightly.

For $\boldsymbol{B}$ ⊥ **c**, illustrated in Fig. 7(d), the A-line is expected to split into two components, with the higher energy component having lower intensity in the PL spectrum due to thermalisation

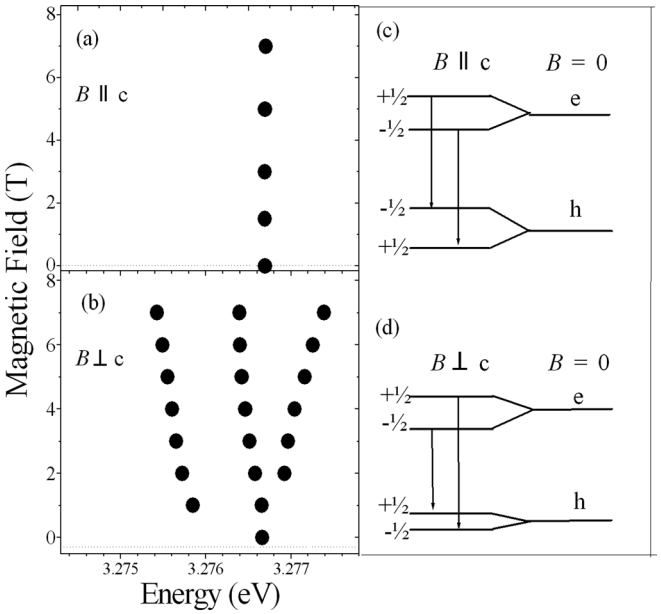

FIG. 7. Variation of the observed line peak energies as a function of magnetic field applied along directions parallel (a) and perpendicular (b) to the c-axis. Schematic diagrams for the case of the A-line emission showing the sign and magnitude of the splitting of the electron and hole spin states under fields parallel (part (c)) and perpendicular (part (d)) to the c-axis.

between the levels. In this case, $g_{eff} = g_e + g_{h\perp}$, and so the splitting is expected to be relatively large since the effects of g_e and $g_{h\perp}$ combine additively. Experimentally, the A-line components are found to separate at a rate of 0.142 meV/T which equates to $g_{eff} = 2.45$, well in excess of that expected for a simple single-particle spin, so if $ge \sim 2$, the value of $g_{h\perp}$ must be well above zero.

The B-line, observed only for non-zero values of $\boldsymbol{B}$ ⊥ **c**, is found to shift to lower energies as $\boldsymbol{B}$ increases, while the two A-line components shift asymmetrically from the zero-field position, with their centre of gravity moving to higher energies as $\boldsymbol{B}$ increases. Such a centre of gravity shift for the A-line could be the result of a diamagnetic shift of the exciton or of interactions between adjacent exciton states. Given that the former is expected to be very small,[18] the observed asymmetry in the shifts of the A-line components from the zero-field position means that interactions are taking place between the $\Gamma_{1,2}$ and $\Gamma_5(\Gamma_3)$ states of the IBX. This is emphatically confirmed by the observation of a strengthening and shifting B-line as the magnetic field $\boldsymbol{B}$ ⊥ **c** increases in magnitude, as shown in Figs. 5 and 6(b). This effect, which has been reported previously for both ionised donor bound exciton (D^+X) and free exciton systems in ZnO,[18,24] is a consequence of the mixing of the $\Gamma_{1,2}$ and $\Gamma_5(\Gamma_3)$ exciton states by a magnetic field applied perpendicular to the c-axis whereby transitions from the $\Gamma_{1,2}$ states (the B-line) acquire some oscillator strength from the $\Gamma_5(\Gamma_3)$ A-line transitions. In this situation, the B:A intensity ratio should depend quadratically on the magnitude of the applied $\boldsymbol{B}$ field, which is indeed the behaviour we have observed (Fig. 6(b)). For an applied field at an arbitrary angle $\theta \neq 90°$ to the c-axis, a splitting of the B-line is expected to be observed,[16] and such angular dependence data are required to provide full confirmation of our analysis. Nevertheless, the weight of

the evidence clearly supports the conclusion that the ZnO:Hg IBX examined here is another example in ZnO of a bound exciton containing a single electron-hole pair having two levels separated by an exchange splitting of roughly 1 meV, where the two levels correspond to the electron and hole having either parallel or anti-parallel spins.

We now turn to considering the g values and whether they support a particular model for the ZnO:Hg IBX. If the impurity centre is electron attractive, then we would expect the highly localised electron to have the pure spin isotropic g value of ~2 and the hole to have a g value typical of a weakly bound ZnO Γ_7 valence band hole. Since for this band the value of $g_{h\perp}$ is close to zero,[25] an estimate of $g_e + g_{h\perp} \sim 2$ is expected for $\boldsymbol{B} \perp \mathbf{c}$ in the case of an electron-attractive impurity centre. On the other hand, if the impurity is hole attractive, then the hole g value could be expected to depart substantially from that of the ZnO Γ_7 valence band,[16] whereas the loosely bound electron g value would be of the order of 1.98, typical of a weakly bound electron in ZnO.[9] The value obtained for $g_{eff} = g_e + g_{h\perp} = 2.45$ certainly favours the latter case. If we assume an isotropic electron g value $g_e = 1.98$, we deduce $g_{h\perp} \sim 0.47$ which is considerably larger than the value of 0.1 obtained for the ZnO:In D^+X bound exciton lines I_2/I_3 by Rodina *et al.*[17]

Overall, our provisional estimates for the ZnO:Hg IBX g values are $g_e \sim 2$, $g_{h||} \sim 2$ and $g_{h\perp} \sim 0.5$. These values are fully consistent with the Hg impurity forming a hole-attractive centre in ZnO. However, it is not safe to argue that as a consequence the IBX is a conventional pseudo-donor since the thermal binding energy obtained from the temperature dependence is only ~12 meV, much less than the spectral binding energy relative to the free exciton position, and also much less than is typical of a shallow donor system in ZnO.[9] The g values for the only other reported case of an IBX centre in ZnO are given as $g_e = 1.97$, $g_{h||} = 1.28$, and $g_{h\perp} = 1.65$.[10] Although these latter values depart to a much greater degree from those of the ZnO valence band[10] compared to the case of ZnO:Hg, the spectral position lies much closer to the free exciton position than does the ZnO:Hg line. Accounting for such differences in IBX properties is a new challenge in ZnO spectroscopy.

V. CONCLUSION

We have undertaken comprehensive radioactive isotope decay, temperature dependence, uniaxial stress, and magneto-optical measurements of the ZnO:Hg PL spectrum in order to determine the nature of the bound exciton giving rise to the luminescence. We have confirmed that the doublet ZPL in ZnO:Hg, with the dominant A-line at 3.2766(1) eV and a much weaker B-line ~0.9 meV lower in energy, results from the recombination of an exciton bound at Hg impurities in the material. The temperature dependence of the PL intensity reveals that the IBX thermal binding energy is ~12 meV, despite its large energy shift of ~100 meV relative to the free exciton position. Uniaxial stress data show that the A-line transitions take place from an orbitally degenerate excited state to a non-degenerate ground state in a centre of trigonal (C_{3v}) symmetry. The magneto-optical properties are characteristic of electron-hole pair recombination at an isoelectronic defect, with the doublet nature of the ZPL luminescence being due to exchange-split $\Gamma_5(\Gamma_3)$ and $\Gamma_{1,2}$ excited states at Hg impurities substituting for Zn in the crystal, consistent with the uniaxial stress data. Although a full angular dependence study, including polarisation measurements, is required in order to provide accurate g values and definitive confirmation of the model, the electron and hole g value estimates obtained in this study indicate that the Hg impurity centre in ZnO is hole-attractive.

The value for the thermal binding energy obtained from the temperature dependence is much less than the spectral binding energy relative to the free exciton position, and also much less than is typical of a shallow donor system in ZnO and the departures of hole g-values (from free hole g-values) determined from Zeeman studies for this defect are also much less than those seen for the only other reported isoelectronic defect in ZnO,[10] which is a more shallow defect. These unusual behaviours run counter to the patterns expected for excitons in materials generally and they may be related to the detailed nature of the defect bonding, reflecting the differing crystal structures of the oxides of Zn and Hg.

ACKNOWLEDGMENTS

This work has been supported by the Science Foundation Ireland Research Frontiers Programme under project 08/RFP/PHY1558 and by the European Community as an Integrating Activity under both the "Support of Public and Industrial Research Using Ion Beam Technology—SPIRIT" (Project No. 227012) and "European Nuclear Science and Applications Research—ENSAR" (Project No. 262010) programmes.

[1]R. Ramesh and V. G. Keramidas, Annu. Rev. Mater. Sci. **25**, 647 (1995).
[2]Z. Yang, C. H. Ko, and S. Ramanathan, Annu. Rev. Mater. Res. **41**, 337 (2011).
[3]A. T. Bell, Science **299**, 1688 (2003).
[4]A. Hagfeldt and M. Grätzel, Acc. Chem. Res. **33**, 269 (2000).
[5]M. Bibes and A. Barthélémy, IEEE Trans. Elec. Devices **54**, 1003 (2007).
[6]P. J. Dean and D. C. Herbert, *in Excitons*, edited by K. Cho (Springer-Verlag, Berlin, 1979), Chap. 3.
[7]J. J. Hopfield, D. G. Thomas, and R. T. Lynch, Phys. Rev. Lett. **17**, 312 (1966).
[8]T. Agne, M. Dietrich, J. Hamann, S. Lany, H. Wolf, T. Wichert, and ISOLDE Collaboration, Appl. Phys. Lett. **82**, 3448 (2003).
[9]B. K. Meyer, H. Alves, D. M. Hofmann, W. Kriegseis, D. Forster, F. Bertram, J. Christen, A. Hoffmann, M. Straßburg, M. Dworzak, U. Haboeck, and A. V. Rodina, Phys. Status Solidi B **241**, 231 (2004).
[10]S. L. Chen, W. M. Chen, and I. A. Buyanova, Phys. Rev. B **86**, 235205 (2012).
[11]J. Cullen, K. Johnston, E. McGlynn, M. O. Henry, D. Dunker, D. R. Yakovlev, and M. Bayer, Phys. Rev. B **87**, 165202 (2013).
[12]C. O'Morain, K. G. McGuigan, M. O. Henry, and J. D. Campion, Meas. Sci. Technol. **3**, 337 (1992).
[13]M. R. Wagner, G. Callsen, J. S. Reparaz, J.-H. Schulze, R. Kirste, M. Cobet, I. A. Ostapenko, S. Rodt, C. Nenstiel, M. Kaiser, A. Hoffmann, A. V. Rodina, M. R. Phillips, S. Lautenschlager, S. Eiserman, and B. K. Meyer, Phys. Rev. B **84**, 035313 (2011).
[14]E. McGlynn and M. O. Henry, Phys. Rev. B **76**, 184109 (2007).
[15]G. F. Koster, J. O. Dimmock, R. G. Wheeler, and H. Statz, *Properties of the Thirty-Two Point Groups* (MIT Press, Cambridge, 1963).
[16]D. G. Thomas and J. J. Hopfield, Phys. Rev. **128**, 2135 (1962).
[17]A. V. Rodina, M. Strassburg, M. Dworzak, U. Haboeck, A. Hoffmann, A. Zeuner, H. R. Alves, D. M. Hofmann, and B. K. Meyer, Phys. Rev. B **69**, 125206 (2004).

[18]L. Ding, C. L. Yang, H. T. He, J. N. Wang, Z. K. Tang, B. A. Foreman, F. Y. Jiang, and W. K. Ge, New J. Phys. **15**, 033015 (2013).
[19]J. L. Birman, Phys. Rev. **114**, 1490 (1959).
[20]Ü. Özgür, Y. Alivov, C. Liu, A. Teke, M. Reschikov, S. Doğan, V. Avrutin, S.-J. Cho, and H. Morkoç, J. Appl. Phys. **98**, 041301 (2005).
[21]J. J. Hopfield and D. G. Thomas, J. Phys. Chem. Solids **12**, 276 (1960).
[22]R. E. Dietz, D. G. Thomas, and J. J. Hopfield, J. Appl. Phys. **32**, 2282 (1961).
[23]M. R. Wagner and A. Hoffmann in *Zinc Oxide—From Fundamental Properties Towards Novel Applications*, edited by C. F. Klingshirn, B. K. Meyer, A. Waag, A. Hoffmann, and J. Geurts (Springer-Verlag, Berlin, 2010), Chap. 8.
[24]B. K. Meyer, J. Sann, S. Lautenschlager, M. R. Wagbner, and A. Hoffmann, Phys. Rev. B **76**, 184120 (2007).
[25]W. R. L. Lambrecht, A. V. Rodina, S. Limpijumnong, B. Segall, and B. K. Meyer, Phys. Rev. B **65**, 075207 (2002).